Carbohydrate Polymers 297 (2022) 120034

Contents lists available at ScienceDirect

Carbohydrate Polymers

journal homepage: www.elsevier.com/locate/carbpol

A novel approach of encapsulating curcumin and succinylated derivative in mannosylated-chitosan nanoparticles

Sourour Idoudi [a], Yousef Hijji [b], Takwa Bedhiafi [a], Hesham M. Korashy [a], Shahab Uddin [c], Maysaloun Merhi [d], Said Dermime [d], Nashiru Billa [a,*]

[a] Department of Pharmaceutical Sciences, College of Pharmacy, QU Health, Qatar University, Doha, Qatar
[b] Department of Chemistry and Earth Sciences, College of Arts and Sciences, Qatar University, Doha, Qatar
[c] Translational Research Institute and Dermatology Institute, Academic Health System, Hamad Medical Corporation, Doha, Qatar
[d] Translational Cancer Research Facility, National Center for Cancer Care and Research, Hamad Medical Corporation, Doha, Qatar

ARTICLE INFO

Keywords:
Curcumin
Succinic anhydride
Mannose
Chitosan nanoparticles
In vitro
Physical

ABSTRACT

Curcumin (CUR) manifests anti-colon cancer activity but suffers from low solubility, bioavailability, and instability, rendering it not as effective as its chemotherapeutic cousins. Here, we conjugate CUR to succinic anhydride (SA), (CUR.SA conjugate), subsequently formulated in mannose-conjugated chitosan nanoparticles (CUR-NPs and CUR.SA-NPs). Instrumental analyses confirmed formation of CUR.SA and mannosylated chitosan (CM) conjugates, with CUR.SA being less crystalline thus, more soluble. Average particle size of CUR-NPs and CUR.SA-NPs were 268 ± 6 nm and 342 ± 4.6 nm, with drug entrapment of 93.34 ± 0.40 % and 98.46 ± 0.06 % respectively. In vitro releases of CUR and CUR.SA from nanoparticles in pH 1.2 and 6.8 media were slow and sustained over 2 h and 72 h, respectively. The physical characteristics of the nanoparticles were unchanged over 3 weeks of storage. Thus, a successful CUR.SA conjugate has been developed, couriered in CM nanoparticles, with favorable attributes that warrant further anti-colon cancer studies, which is ongoing.

1. Introduction

Curcumin (CUR), or diferuloylmethane, is a diaryl heptanoid curcuminoid and the principal component in turmeric, *Curcuma longa* Linn (Willenbacher et al., 2019). The other curcuminoids found in turmeric are demethoxycurcumin and bis-demethoxycurcumin (Lestari & Indrayanto, 2014). CUR was first isolated from turmeric oil and resin by Pelletier and Vogel in 1948 (Rodrigues, Anil Kumar, & Thakur, 2019), and its structure was fully elucidated a decade later (Upadhyay, Gautam, Ramu, Kondaiah, & Chakravarty, 2019). It has a melting point of 183 °C and a molecular mass of 368.37 g/mol (Mbese, Khwaza, & Aderibigbe, 2019). Turmeric powder is used as a spice and an herb for the treatment of injuries, stress, depression, infections and skin diseases (Willenbacher et al., 2019; Zheng & Mcclements, 2020). It has antioxidant, antimicrobial, anti-inflammatory, and anti-tumor activities (Hao et al., 2020). In spite of these therapeutic activities, the usage of CUR is impeded due to low aqueous solubility and instability, resulting in poor systemic bioavailability (Mbese et al., 2019). On the other hand, CUR is well-tolerated in high doses and pharmacologically safe (Asher & Spelman, 2013).

Structural modification of CUR through chemical conjugation with relevant functional groups may potentially yield derivatives with supra-potent activity to CUR (Tomeh, Hadianamrei, & Zhao, 2019). For example, succinylation of CUR has been shown to enhance its anti-cancer activity (Wichitnithad, Nimmannit, Wacharasindhu, & Rojsitthisak, 2011). It is also possible to modify the physicochemical properties of CUR to address its low instability in alkaline media and poor solubility through novel formulation interventions. In this regard, nano-encapsulation in diverse carriers including liposomes (Yi et al., 2018), microspheres (Saranya, Rajan, Biswas, Jayakumar, & Sathianarayanan, 2018), micelles (Le & Kim, 2019), and polymeric nanoparticles is achievable (Valencia et al., 2021). Arguably, chitosan has been the subject of much interest by researchers in the quest for improved delivery of drugs and clinical outcomes from drugs that manifest poor systemic bioavailability. Chitosan (CS) is an *N*-deacetylated derivative of chitin obtained from the shells of marine crustaceans (Song, Lee, Tan, & Li, 2019). Furthermore, CS is biocompatible and has been used to formulate drug delivery systems that improve the cellular uptake of

* Corresponding author at: Pharmaceutical Sciences Department, College of Pharmacy, Qatar University, Qatar.
E-mail address: nbilla@qu.edu.qa (N. Billa).

https://doi.org/10.1016/j.carbpol.2022.120034
Received 14 July 2022; Received in revised form 21 August 2022; Accepted 22 August 2022
Available online 24 August 2022

several therapeutics (Aibani, Rai, Patel, Cuddihy, & Wasan, 2021). Of relevance to the current work is that CS polymeric nanoparticles have been shown to be essential in protecting CUR from degradation, promoting cellular uptake, thereby potentiating its therapeutic activity (Baskaran, Madheswaran, Sundaramoorthy, Kim, & Yoo, 2018). Furthermore, conjugation of CS with mannose (mannosylated-CS) and formulation as nanoparticles has been shown to prompt effective uptake of the nanoparticles by cancer tissue (Shi et al., 2017). Mannose is a monosaccharide available in small amounts in some fruits (Domenici et al., 2016; Tang, 2017), and its receptors are highly expressed within cancer cells, which promotes uptake of mannosylated nanoparticles (Xiong et al., 2017). In this context, we aimed to study the physical properties of succinylated-CUR (CUR.SA) encapsulated within mannosylated-CS nanoparticles in comparison to unconjugated CUR. This study serves as a premise for biological evaluation of the CUR.SA, which is currently being conducted.

2. Materials and methods

2.1. Materials

Curcumin (mixture of curcumin 98 %, with demethoxycurcumin, and bisdemethoxycurcumin, CAS: 458-37-7) and chitosan (MW: 100.000–300.000 kDa, CAS: 9012-76-4) were purchased from Acros Organics. D-Mannose (CAS: 3458-28-4), 4-(dimethyl amino) pyridine (≥98 %, CAS: 1122-58-3), ethanol (≥99.8 %), methanol (>99.9 %, HPLC gradient), acetonitrile (>99.9 %, HPLC gradient) and acetic acid were purchased from Honeywell Fluka. Succinic anhydride (≥99 %, CAS: 108-30-5), sodium triacetoxyborohydride CAS: 56553-60-7), and chloroform were purchased from Sigma Aldrich. Sodium tripolyphosphate (STPP) (Granular, CAS: 7785-84-4) was purchased from Alfa Aesar. Diethyl ether (≥98 %) and ethyl acetate ≥99.5 % were purchased from VWR. Other chemicals and solvents used were reagent grade and used as directed.

2.2. Synthesis of chitosan-mannose conjugate

Chitosan-mannose conjugate (CM) was synthesized via reductive amination as described in the literature (Chaubey et al., 2018; Ejaz, Ihsan, Noor, Shabbir, & Imran, 2020), with some modifications (Fig. 1A). Briefly, chitosan (160 mg) was mixed with D-mannose (16 mg) in 1 % acetic acid and pH adjusted to 5.5 with 2 M NaOH with addition of sodium triacetoxyborohydride ($NaBH(OAc)_3$) to reduce the intermediate imine. The obtained solution was stirred at 210 rpm at room temperature for 48 h and CM precipitated out using 2 M NaOH and separated by centrifugation at 4000 rpm for 10 min. The pellet was washed with deionized water twice (centrifuged and supernatant discarded). Finally, the pellet was dried at 40 °C in an oven overnight.

2.3. Synthesis of curcumin-succinic anhydride conjugate

CUR-succinic anhydride (CUR-SA) conjugate was synthesized according to Fig. 1B. Briefly, a 1:2 ratio of CUR and SA was completely dissolved in chloroform (containing dimethyl amino pyridine (DMAP) as a catalyst), and stirred at 400 rpm at room temperature for 4 h. Excess solvent was removed by rotary evaporation at 70 °C. Formed CUR-SA was washed with diethyl ether, dissolved in ethanol, and dried overnight at 25 °C.

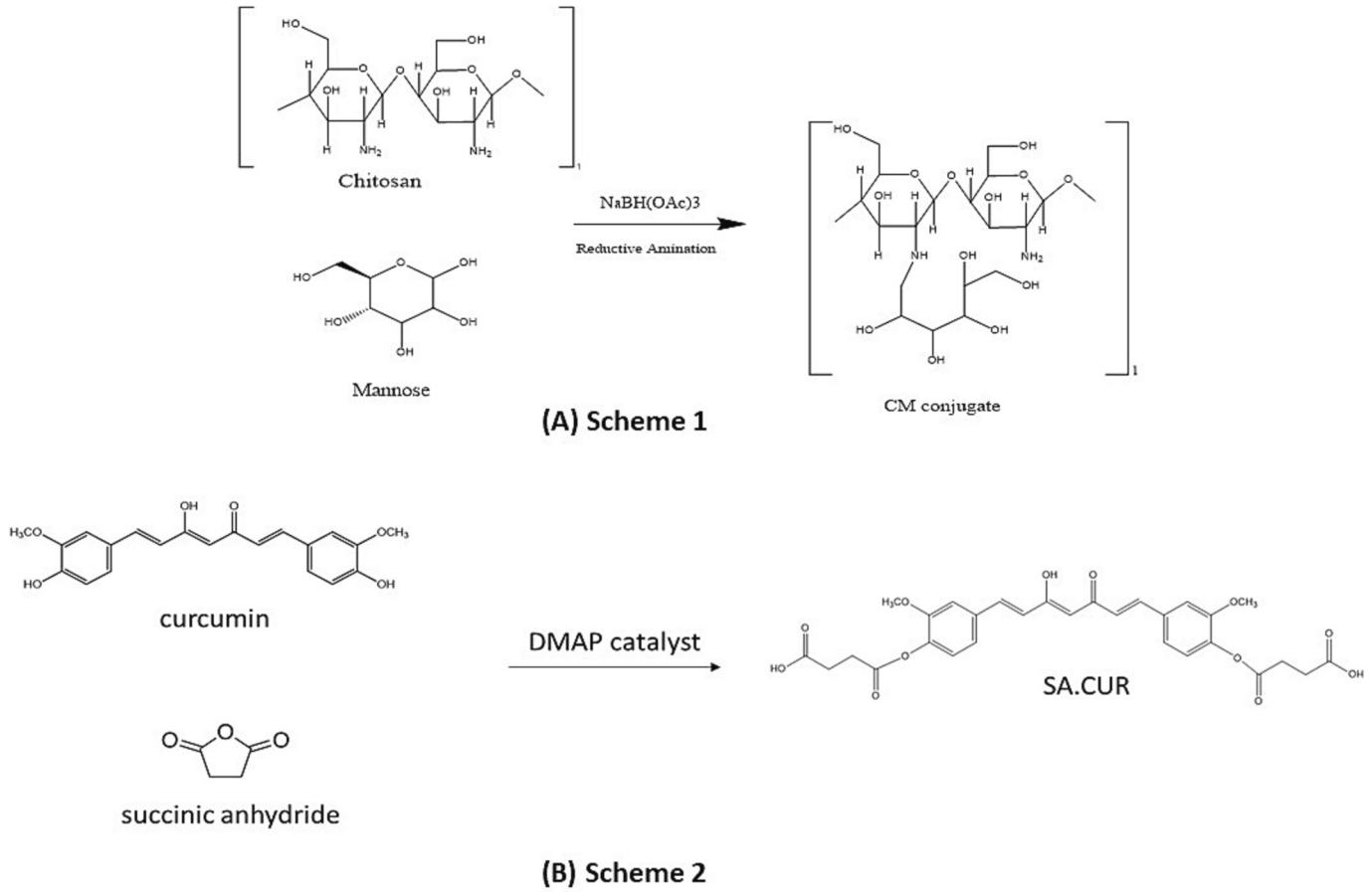

Fig. 1. (A) Scheme 1: conjugation of chitosan to mannose (CM); (B) Scheme 2: conjugation of curcumin to succinic anhydride (CUR.SA).

2.4. Formulation of CUR.SA -loaded CM nanoparticles

A 100-μL aliquot of (STPP) (1 mg/mL) solution was added dropwise to a mixture of 1 mL CM solution (2 % (V/V) in acetic acid) and 1 mL of CUR.SA (1 mg/mL in ethanol). The mixture was stirred for 30 min followed by centrifugation at 4000 *g* for 15 min and the supernatant transferred to Eppendorf® microcentrifuge tubes for subsequent analysis. Blank mannosylated chitosan nanoparticles (CM-NPs) and curcumin encapsulated mannosylated-chitosan nanoparticles (CUR-NPs) were similarly formulated.

2.5. HPLC assay for CUR

An HPLC system (series 1260, Agilent, USA), equipped with a UV/Vis detector (G1315C, Agilent, USA) set at 425 nm was used for CUR analysis. The stationary phase comprised of a reverse-phase column (XBridge UPLC Waters, 150 mm × 3 mm, 2.5 μm, USA) and the mobile phase; methanol:0.01 % acetic acid:acetonitrile (5:43:52 %), run at 0.3 mL/min, with an injection volume of 5 μL.

2.6. Stability of CUR and CUR.SA

Solutions of CUR and CUR.SA conjugate, prepared in ethanol, were exposed to darkness, roomlight, or sunlight, each for 0.5, 1, 2, 4, and 6 h and the amount of CUR or CUR.SA remaining at each time was assessed using the HPLC system described in Section 2.5.

2.7. Solubility of CUR and CUR.SA

The aqueous solubility of CUR and CUR.SA conjugate was determined by adding excess amount of each in ultra-pure water and stirred at 300 rpm for 24 h at ambient temperature until saturation equilibrium. A 1 mL aliquot of each saturated solution was filtered through a 0.2 μm pore membrane filter and a 1:1 mixture with methanol was injected on to the HPLC system as described in Section 2.5. The solubility of CUR and CUR.SA in ethanol was similarly determined.

2.8. Chemical constituents of conjugates and nanoparticles

FT-IR analyses on CUR, CS, mannose, SA, CUR.SA conjugate, CM conjugate, STPP, CM-NPs, CUR-NPs, and CUR.SA-NPs were conducted by recording absorption spectra between 4000 cm^{-1} and 400 cm^{-1} on a Spotlight 400 FTIR Spectrophotometer (Perkin Elmer, USA). Further analyses based on ^{1}H and ^{13}C NMR spectroscopy were conducted on CUR, CS, mannose, SA, CM, and CUR.SA conjugates using a JNM-ECZR (600 MHz) FT Spectrometer (JEOL, USA). Chemical shifts were recorded in parts per million (ppm) relative to the solvent peak and the coupling constant (*J*) and recorded in Hertz (Hz).

2.9. Zeta average and potential of nanoparticles

The particle size, polydispersity index (PDI) and zeta potential analyses were conducted on a Zeta sizer Nano ZS (Malvern Instruments, UK). All data are presented as mean ± SD (n = 3).

2.10. Estimation of encapsulation parameters

To estimate the percentage encapsulation efficiency (%EE) of drug loaded within the nanoparticles, the supernatant from the centrifuged CUR-NPs and CUR.SA-NPs formulations were assayed for free CUR or CUR.SA, respectively, and analyzed by HPLC (Section 2.5). Detector responses from HPLC analyses of samples from the supernatant were compared to a standard calibration to deduce the concentration of non-encapsulated CUR or CUR.SA. The % EE was subsequently computed using Eq. 1 and the drug loading (DL) using Eq. 2.

$$\%EE = \frac{\text{Initial amount of CUR or CUR.SA} - \text{free CUR or CUR.SA)}}{\text{Initial amount of CUR or CUR.SA}} \times 100\% \quad (1)$$

$$\%DL = \frac{\text{Weight of drug in the nanoparticles}}{\text{Weight of the nanoparticles}} \times 100\% \quad (2)$$

2.11. Morphological and elemental analyses of the nanoparticles

The morphology of the nanoparticles was examined on a Nova Nano (SEM) equipped with an EDX detector (Model Nova Nano SEM 450, ThermoFisher Company, USA). Two drops of the nanoparticles were deposited on the SEM stub to the air-dry followed by scanning on SEM operated at 5 kV. Further morphological analyses were conducted on the nanoparticle using an atomic force microscope (AFM), (MFP3D, Asylum Research UK). Samples were air-dried on freshly cleaved mica sheets and mounted on the AFM platform with double-sided adhesive. The cantilever was operated at a force constant of 0.7 $N{\cdot}m^{-1}$, resonance frequency of 150 kHz in scanning, and nano indentation mode over a scan area of 5 × 5 μm. EDX analyses were conducted on the nanoparticles in order to study the elemental composition of CS, STPP, CM-NPs, CUR-NPs and CUR.SA-NPs.

2.12. Crystallographic analyses on conjugates and nanoparticles

Crystallographic analyses on samples (CS, mannose, CM conjugate, CUR, SA, CUR.SA conjugate, CM-NPs, CUR-NPs, and CUR.SA-NPs) were conducted using X-ray diffractometer (PANalytical, Netherlands) operated at 45 kV and 40 mA with scan angles from 5 to 75° and scanning speed of 0.02°/step to a complete step time of 0.5 s.

2.13. Drug release from nanoparticles

Drug release from the nanoparticles was determined by dispersing 1 mL of nanoparticles suspension in pH 1.2 (0.1 N HCl) or pH 6.8 (PBS) in a 2:1 (v/v) suspension to media ratio. 500 μl aliquots of each suspension were distributed in ten Eppendorf® tubes maintained at 37 °C in an incubator under shaking at 150 rpm. For CUR or CUR.SA conjugate release in pH 1.2 medium, three tubes were withdrawn at predetermined time intervals of 0 (initial), 1, and 2 h, centrifuged at 14,000 rpm to separate the released CUR or CUR.SA conjugate from the nanoparticles (pellet form). Similarly, CUR or CUR.SA release in pH 6.8 medium were obtained at 0 and 1, 4, 6, 24, 48, and 72 h. The released drug was mixed with ethanol, filtered, and injected into the HPLC system (Section 2.5). The percentage of drug released was estimated using Eq. 3. Data are expressed as the mean of three independent runs.

$$\%Amount\ of\ CUR\ released = \frac{Amount\ of\ CUR\ or\ CUR.SA\ released}{Total\ CUR\ or\ CUR.SA\ in\ NPs} \times 100\% \quad (3)$$

2.14. Physical changes in nanoparticles as a function of storage

The physical changes (hydrodynamic diameter, PDI, and zeta potential of the nanoparticles) in the CUR-NPs, and CUR.SA-NPs over one month storage at 4 and 37 °C were determined at 0, 1, 7, 14 and 28 days (Valencia et al., 2021).

2.15. Statistical analyses

All data are expressed as mean ± SD of replicates from independent assays (n = 3). Statistical significance of the data was determined using a one-way ANOVA and Student's *t*-test, as necessary, using a GraphPad Prism 9 software with significant difference indicated at p-values < 0.05.

3. Results and discussion

3.1. Chemical composition of conjugates and nanoparticles

FT-IR absorption band at 1585.2 cm^{-1} (Fig. 2A) can be assigned to the stretching vibration of the $–NH_2$ group present in CS, whilst 1022.09 cm^{-1} is attributable to C—O stretching vibration (Fig. 2A). The spectrum for mannose (Fig. 2A) shows two characteristic peaks at 3293.82 cm^{-1} and 3127.97 cm^{-1}, similar to the C—H vibrational stretching. CM conjugate shows a strong sharp peak at 1554.34 cm^{-1}, which is due to bending of the secondary amine of CS (N—H) at 1407.78 cm^{-1} bonded to mannose ligand. Moreover, an intense broad peak at around 3200 cm^{-1} found in the spectrum of the CM is due to –OH groups in mannose, confirming the presence of mannose in the conjugate. Similar findings were observed in the literature (Chaubey & Mishra, 2014). A C═C aromatic stretch vibration at 1427.07 cm^{-1} (Fig. 2B) and high intensity band at 1500.35 cm^{-1} refer to mixed vibrations including those coming from carbonyl bond (C═O) of CUR. In CUR. SA, a strong peak at 1774.19 cm^{-1} due to C═O of CUR stretching was observed (Fig. 2B), pointing to the formation of the CUR.SA conjugate. Furthermore, the phenolic ring stretch vibration (O—H) in CUR occurring at 3600 cm^{-1} is disappeared in CUR.SA (Petković, 2012). CUR.SA has no phenolic OH groups. In the nanoparticles: CM-NPs, CUR-NPs and CUR.SA-NPs, key signatures observed previously are also present as shown in Fig. 2C, however, representative peaks appeared smoothened and slightly shifted, attributable to amorphous transformation of CUR and CUR.SA in the nanoparticles and formation of ionic interactions between STPP and CS during gelation.

^{1}H NMR analyses on CS and CM conjugate are presented in Fig. 3A and C respectively. Signals between 3.60 and 3.90 ppm correspond to protons in the glucopyranose ring bonded to C atoms, which are overlapped (Fig. 3A). Peaks at 1.90 and 3.00 ppm represent protons from CS bonded to C atoms within the glucosamine ring, similarly to previous observations (Chaubey et al., 2018). In the present investigation, mannosylation of CS present a weak peak at 2.63 ppm, attributable to proton linked –NH group of CS, which confirms the formation of secondary amino groups (Fig. 3C). Moreover, a peak at 8.14 ppm occurs only in the CM conjugate (in contrast to CS) and is attributable to protons from mannose. Other representative peaks in CS are shifted in CM, which is a strong indication of mannosylation of CS.

^{13}C NMR analyses of free CUR and CUR.SA are shown in Fig. 3D and F, respectively. Peaks at 172 ppm and 173 ppm emerged from carbonyl and carboxylic acid groups in SA and hence the CUR.SA conjugate (Fig. 3F). These peaks are evidently absent from CUR (Fig. 3D). Furthermore, a peak at 30 ppm represents C in the $–CH_2$ groups within SA. This peak is also absent in CUR. Other relevant peaks found in the conjugates (CUR.SA and CM) are also reported in the literature (Asthana, Asthana, Kholi, & S. V., 2021; Chaubey et al., 2018; Chaubey, Patel, & Mishra, 2014). After encapsulation in the mannosylated-CS nanoparticle carrier (CM) system, the presence of both CUR and CUR. SA within the nanoparticles was confirmed by FT-IR and NMR (data not shown) and corroborated with those in the literature (Ejaz et al., 2020; Nair, Morris, Billa, & Leong, 2019). We may conclude that CUR was successfully conjugated to SA and encapsulated in CM.

3.2. Physicochemical properties of CUR and CUR.SA conjugate

Plots of concentration versus time profiles of CUR and CUR.SA conjugate (Fig. 4A & B) showed no significant differences in degradation of the two drugs in dark and room light ($p > 0.05$) after 6 h of exposure. On the other hand, a significant difference in degradation was observed after 6 h of sunlight exposure ($p < 0.0001$). This can be explained by the instability and photodegradable profiles of CUR when it is exposed to sunlight. Photodegradation of CUR and by extension CUR.SA, is preceded by demethoxylation and isomerization of the keto-enol configuration to the di-keto form with the formation of side products such as

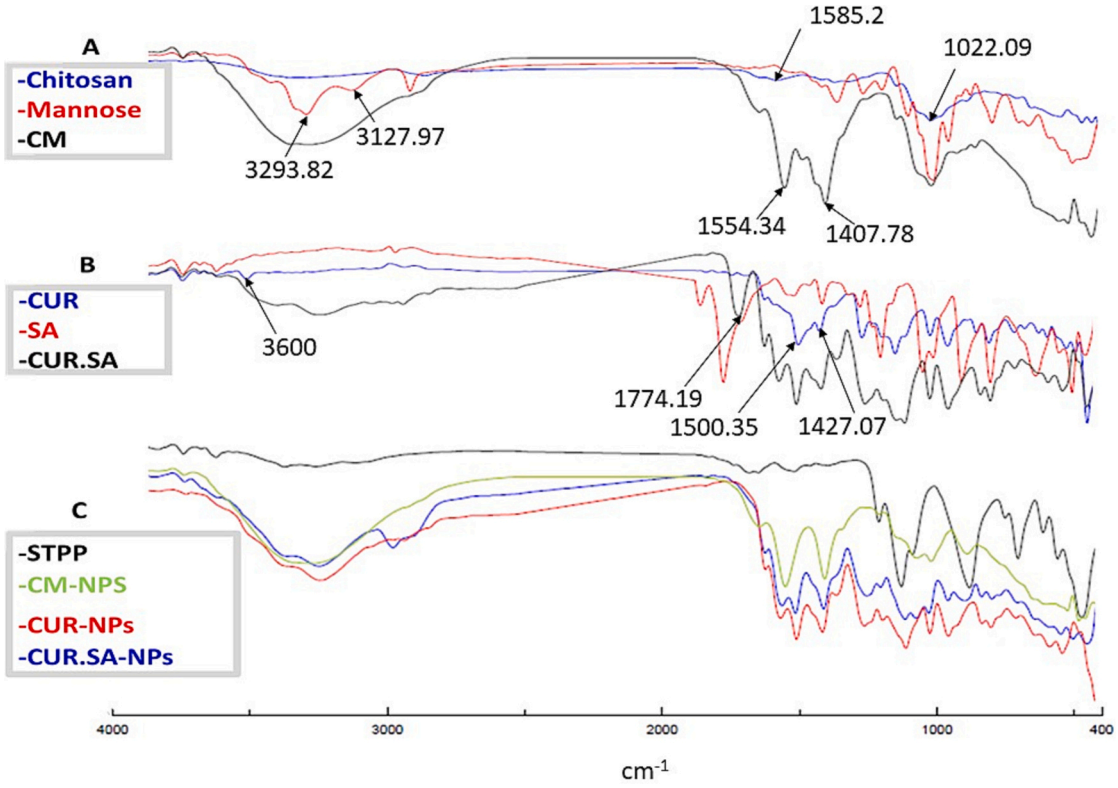

Fig. 2. FT-IR spectra of (A) chitosan, mannose and CM conjugate; (B) curcumin (CUR), succinic anhydride (SA), and curcumin-succinate conjugate (CUR.SA); (C) sodium tripolyphosphate (STPP), mannosylated chitosan nanoparticles (CM-NPs), curcumin in mannosylated chitosan nanoparticles (CUR-NPs), and curcumin-succinic anhydride conjugate in mannosylated chitosan nanoparticles (CUR.SA-NPs).

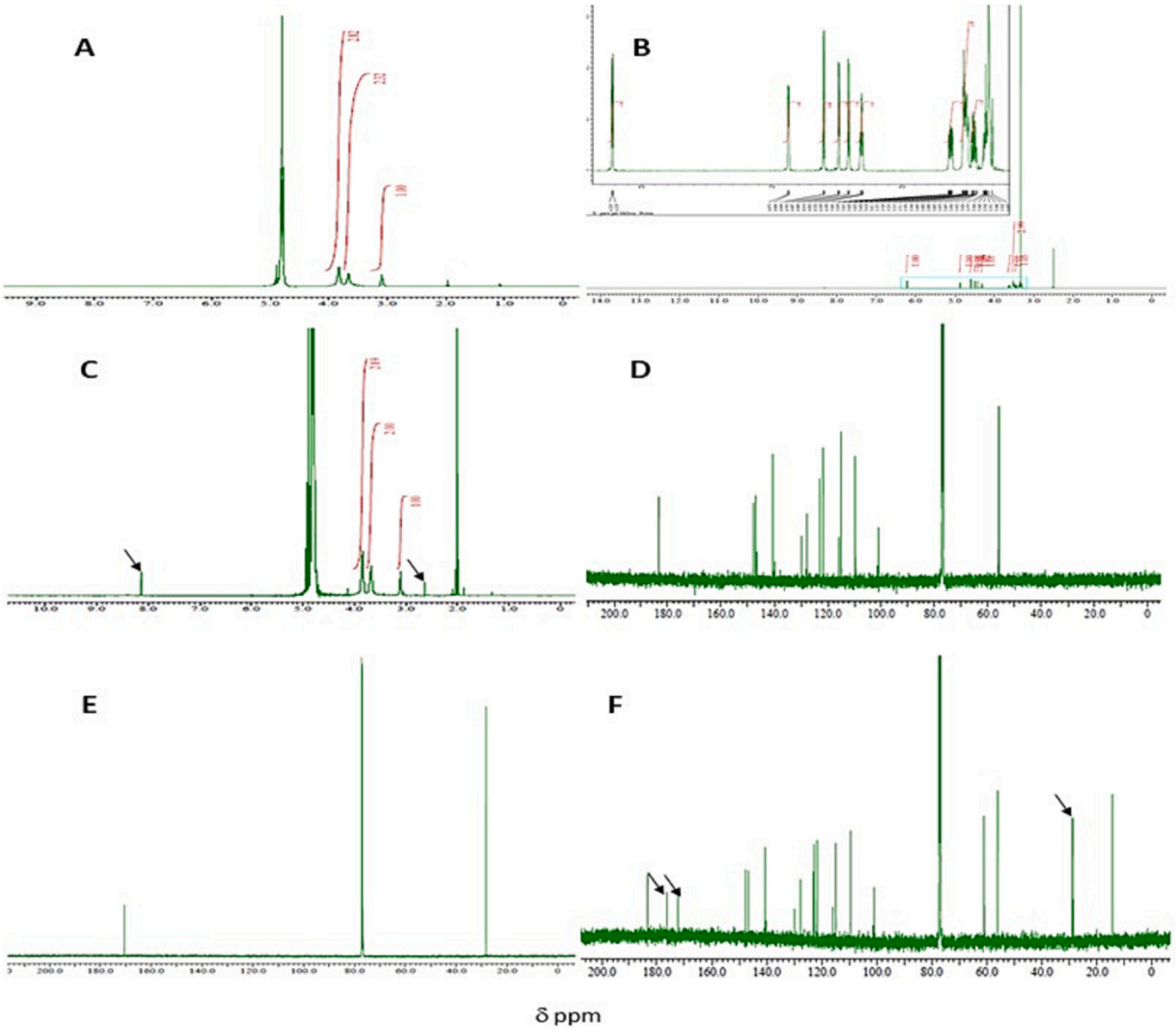

Fig. 3. ^{1}H NMR spectra of (A) CS; (B) Mannose; (C) CM conjugate in D_2O/HCl; ^{13}C NMR spectra of (D) CUR; (E) SA; (F) CUR.SA in deuterated chloroform ($CDCl_3$).

methanol or acetate (Del Castillo, López-Tobar, Sanchez-Cortes, Flores, & Blanch, 2015). The gradient of the CUR.SA degradation profile in light (Fig. 4B) is steeper than the CUR degradation profile in light (Fig. 4A), suggesting that the CUR.SA is less stable than CUR. Solubility assessment of CUR and CUR.SA in aqueous and ethanolic media (Fig. 5) indicates that CUR was more soluble than CUR.SA conjugate ($p < 0.05$) in ethanol. However, CUR.SA conjugate showed a higher solubility in water compared to free CUR ($p < 0.05$). The improved solubility is attributable to the presence of succinic acid moieties, which are hydrophilic. Thus, overcoming these physicochemical constraints are likely to impact positively the therapeutic outcomes of CUR (Sorasitthiyanukarn, Muangnoi, Rojsitthisak, & Rojsitthisak, 2021).

3.3. Physical properties of nanoparticles

The mean size of the empty carrier (CM-NPs) was 101 ± 4.3 nm, with a PDI of 0.32 ± 0.05, and a zeta potential of 41.2 ± 0.15 mV. The mean size of CUR-NPs was larger (268 ± 6 nm), with a PDI of 0.294 ± 0.019 and a zeta potential of 11 ± 0.75 mV. For the encapsulated conjugate (CUR.SA-NPs), the size was highest (342 ± 4.6 nm), with a PDI of 0.137 ± 0.043 and zeta potential of 13.6 ± 0.8 mV. Due to its excellent crosslinking functionality and nontoxicity, STPP has been widely used to formulate CS nanoparticles (Ficai, Albu, Sonmez, Ficai, & Andronescu, 2016; Tarhini, Badri, Greige-Gerges, Fessi, & Elaissari, 2021). Medium MW CS has previously been used to encapsulate CUR, but resulted in the formation of microparticulate (Pooresmaeil & Namazi, 2020). The method employed in the present study produced nanoparticles of relevant size range with regard to uptake by cancer cells. The larger size observed with CUR.SA-NPs is attributable to the increased size of the conjugate due to the two succinyl moieties on CUR. The lower zeta potential observed in CUR-NPs and CUR.SA-NPs as opposed to CM-NP is indicative of possible interaction between the payloads (CUR/CUR.SA conjugate) and free NH_2 groups of CS. The % EE was 93.34 ± 0.40 for CUR-NPs, and 98.46 ± 0.06 for CUR.SA-NPs, whilst the % drug loading was 39.81 ± 0.17 % for CUR-NPs, and 42.02 ± 0.02 % for CUR.SA-NPs. The data is comparable to CUR %EE from previous studies (Ahmadi et al., 2017; Chaubey et al., 2014; Kamaraj et al., 2018).

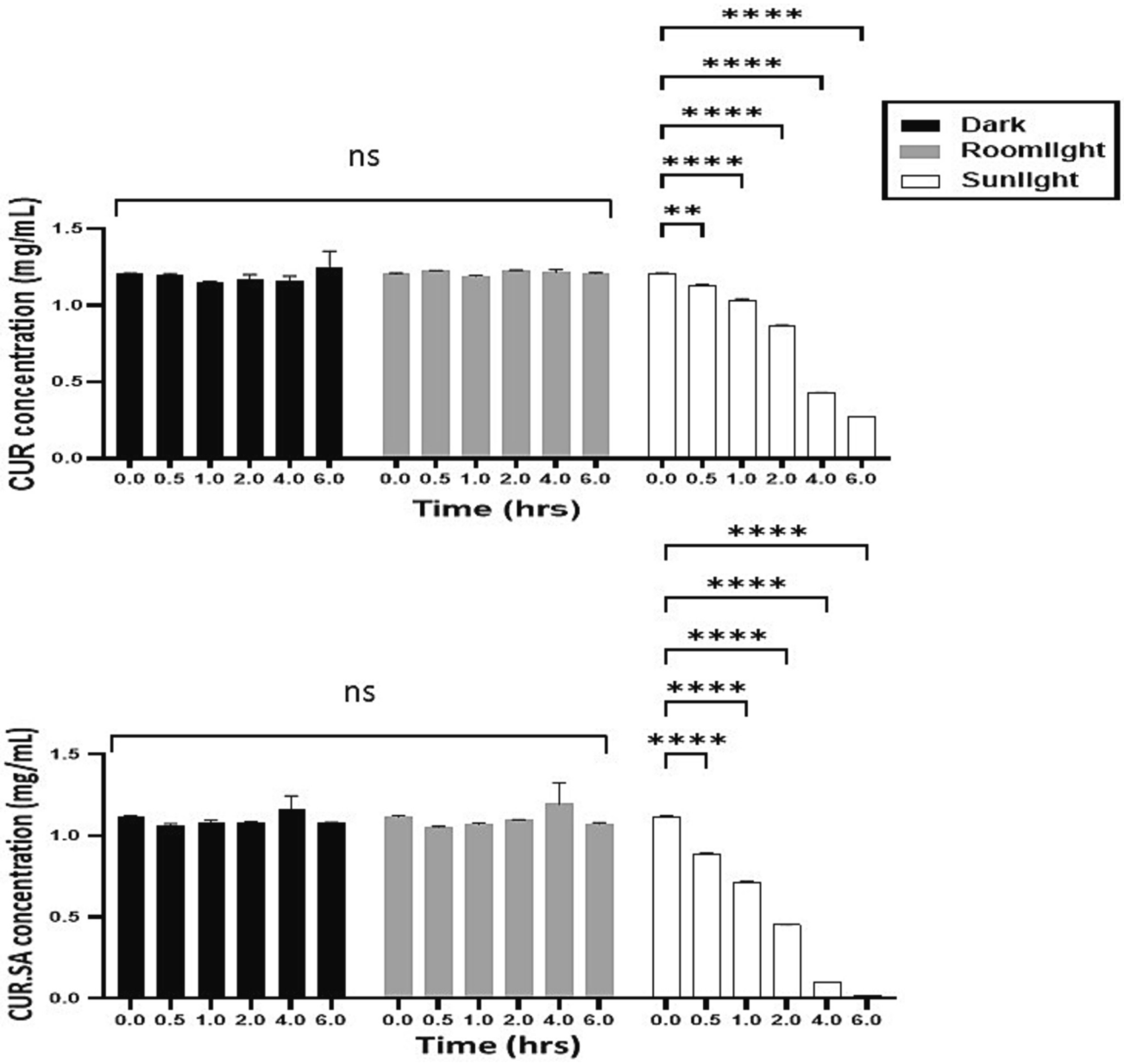

Fig. 4. Photostability of (A) free CUR; (B) CUR.SA conjugate. Data expressed as mean ± SD ($n = 3$), compared by two-way ANOVA, followed by Dunnett's test, (ns = not significant, * $p < 0.05$, ** $p < 0.01$ and *** $p < 0.001$, and **** $p < 0.0001$ indicate statistical significance compared to control (time 0)).

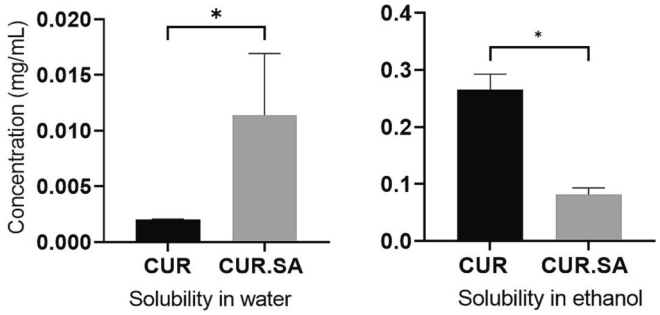

Fig. 5. Solubility of CUR and CUR.SA conjugate in water and ethanol. Data expressed as mean ± SD (n = 3). Statistical significance (*) indicated at $p < 0.05$, using Student's *t*-test.

3.4. Morphological and surface topographic analyses of nanoparticles

SEM images of the blank, CUR or CUR.SA loaded nanoparticles appear spherical and discrete (Fig. 6A), with the range in agreement with the DLS data. The discreteness of the particles is an indication that sufficient surface charge was retained within the particles. Elemental (C, O, N, Na, P) analyses on the nanoparticles using EDX-linked SEM revealed the presence of Na and P, an indication of crosslinking between CS and STPP (Table 1). EDX is a surface analysis, thus, the data suggest the formation of a CS-STPP matrix, within which CUR is amorphously distributed (Nair et al., 2019; Villegas-Peralta et al., 2021).

Fig. 6 also displays AFM 2D and 3D rendered images of CM-NPs (D), CUR-NPs (E), and CUR.SA-NPs (F), with spherical nanoparticles uniformly distributed. The average surface roughness ranged between −13.590 nm and 27.109 nm for CM-NPs (Skewness = 0.34 nm) (G); −13.801 nm and 21.792 nm for CUR-NPs (Skewness = 0.57 nm) (H); and −36.602 nm and 74.815 nm for CUR.SA-NPs (Skewness = 2.91 nm) (I). These are indicative of a smooth surface, whilst the observed

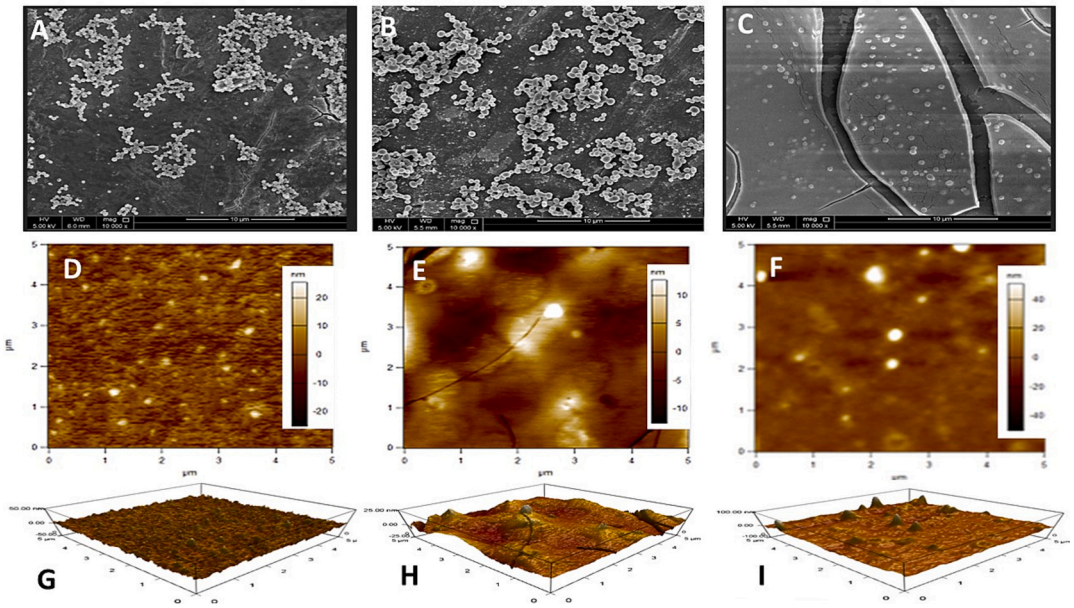

Fig. 6. SEM images of (A) CM-NPs; (B) CUR-NPs; (C) CUR.SA-NPs and AFM images of: (D) CM-NPs; (E) CUR-NPs; (F) CUR.SA-NPs with 3D rendered AFM images of (G) CM-NPs; (H) CUR-NPs; (I) CUR.SA-NPs.

Table 1
Elemental composition of samples (wt%).

Sample	% N	% O	% C	% Na	% P
CS	18.01	27.91	54.08	–	–
STPP	–	49.11	–	28.48	22.41
CM-NPs	27.40	32.02	34.22	4.91	1.45
CUR.SA-NPs	26.59	27.83	36.16	9.04	0.38
CUR-NPs	18.80	24.51	51.53	4.68	0.48

roughness is much lower than that of the plane size of nanoparticles. Such sphericity of CS nanoparticles has been also reported in the literature (Chaubey et al., 2018; Samrot, Burman, Philip, Shobana, & Chandrasekaran, 2018; Xiao, Nian, & Huang, 2015), however, the discreteness was not always associated with the sphericity.

3.5. Crystallographic analysis of CUR and CUR.SA nanoparticles

Several sharp spikes ascribable to crystalline signals in CUR disappear on conjugation to SA, again, an indication of decreased crystallinity of CUR.SA, which correlates with CUR.SA presents a better solubility than CUR in aqueous media (Fig. 7). Two strong peaks at $2\theta = 10.5^{\circ}$ and

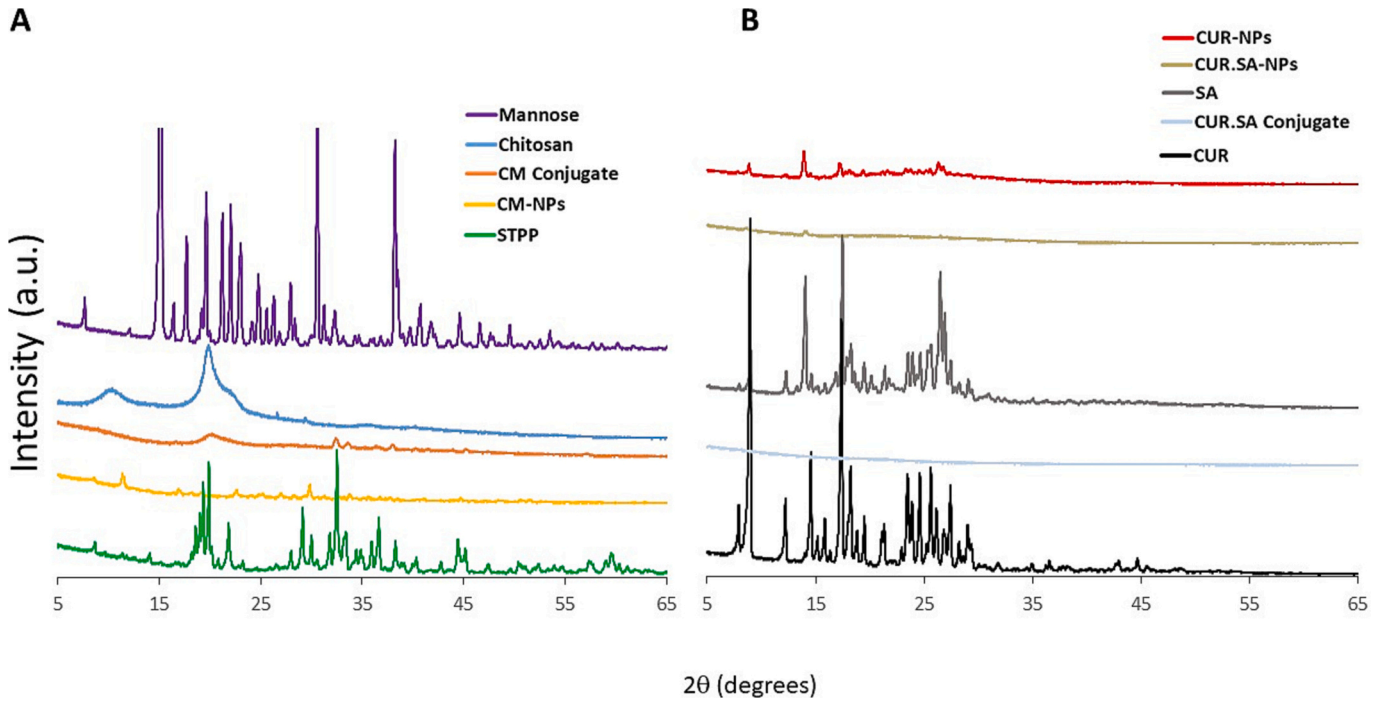

Fig. 7. XRD scans of (A) mannose, chitosan, CM conjugate, CM-NPs and STPP; (B) CUR-NPs, CUR-SA-NPs, SA, CUR-SA conjugate and CUR.

20.43° were observed in CS diffraction patterns, which on mannosylation causes 10.5° to disappear and 20.43° to decrease in intensity. In CM-NPs, both peaks disappear completely, which is an indication of transformation to an amorphous configuration. Encapsulation of CUR or CUR.SA within CM-NPs resulted in the disappearance of most of the sharp peaks observed particularly with CUR. This represents a transformation of CUR and CUR.SA into the amorphous configuration during encapsulation. Amorphous manifestation ensures improved solubility, which is desirable in the present circumstance since deployment in the cells will promote effective therapeutics. Reduced crystallinity reflects improved dissolution rate due to a decrease in the lattice-free energy (Babu & Nangia, 2011). The data is supported by previous studies where a reduction in crystallinity was also reported after encapsulation of CUR in CS polymeric nanocarriers (Dhanasekaran, Rameshthangam, Venkatesan, Singh, & Vijayan, 2018; Han, Chen, Gao, Zhang, & Tang, 2020; Ubeyitogullari & Ciftci, 2019).

3.6. Drug release from prepared nanoparticles

CUR and CUR.SA-release from the nanoparticles at pH 1.2 and pH 6.8 are presented in Fig. 8A and B respectively. A burst CUR release was observed in the first 2 h of up to 30 % in pH 1.2 and pH 6.8, followed by a constant and slow release up to 72 h in pH 6.8. CUR.SA release in pH 1.2 and 6.8 (Fig. 8B) followed a similar profile as CUR, albeit slightly higher. The slow release of CUR and CUR.SA represents a protective property of the carrier. However, the release of CUR and CUR.SA was slightly higher at pH 1.2 compared to pH 6.8, attributable to the solubility of CS in acidic media. Drug release studies gives us some idea of how much of the cargo is retained within the nanoparticles prior to cellular uptake. In this regard, we note that none of the formulation released >40 % of cargo over the 72 h study, suggesting a significant drug retention within the CM carrier. Such slow release profiles observed in the present study is desirable in cancer therapy (Kumari et al., 2021). Although the scope of this report does not include antitumor studies, it is noteworthy that since the average pH of tumors is 6.7–7.4, we may infer that the release of the drugs from the nanoparticles within tumor may follow a similar sustained profile. An anticancer cell study is currently underway to ascertain this assertion.

3.7. Physical properties of nanoparticles as a function of storage

Storage is a key stability-indicating parameter in formulations and changes in physical properties during storage can be used to ascertain the stability of the formulation as a function of time. This is especially true for nanoformulations. During storage, variations in the size, zeta potential, and PDI could take place and the nanoparticles become aggregated. Assessment of the physical characteristics of CUR-NPs and CUR.SA-NPs during storage at 4 °C and 37 °C showed that no significant changes in size of the nanoparticles was observed after 28 days at 4 °C (Fig. 9A & B). In contrast, significant increases were observed at 37 °C on day 28 (539 ± 15 nm and 536 ± 2 nm for CUR-NPs and CUR.SA-NPs, respectively) compared to sizes on other days. Furthermore, the PDI was <0.5 at both storage conditions with no differences observed between their means ($p > 0.05$) for both types of nanoparticles. The zeta potential of CUR-NPs and CUR.SA-NPs retained a positive magnitude at both temperatures. Thus, the nanoformulations exhibit a temperature-dependent stability pattern.

4. Conclusion

CUR is reported to possess anticancer properties; however, this property is impeded due to it low solubility. The present work aimed to address the low solubility of CUR through i) conjugation of SA to CUR and ii) encapsulation in mannose-conjugated CS nanoparticles, as mannose receptors are being highly expressed in cancer cells. The CUR.SA conjugate and subsequent encapsulation in CM nanoparticles presented desirable physical and stability characteristics, based upon which we project that CUR.SA encapsulated CM nanoparticles will present supra anticancer properties to CUR, thus setting the stage for subsequent cell work, which is on-going, to ascertain the therapeutic effectiveness of CUR.SA.

CRediT authorship contribution statement

Sourour Idoudi: Data curation, Formal analysis, Writing - original draft. **Yousef Hijji:** Supervision, Writing – review & editing. **Takwa Bedhiafi:** Formal analysis. **Hesham M. Korashy:** Supervision. **Shahab Uddin:** Supervision, Writing – review & editing. **Maysaloun Merhi:** Supervision, Writing – review & editing. **Said Dermime:** Supervision. **Nashiru Billa:** Conceptualization, Main Supervision, Validation, Funding acquisition, Methodology, Project administration, Resources, Writing - review & editing.

Declaration of competing interest

The authors declare that they have no known competing financial

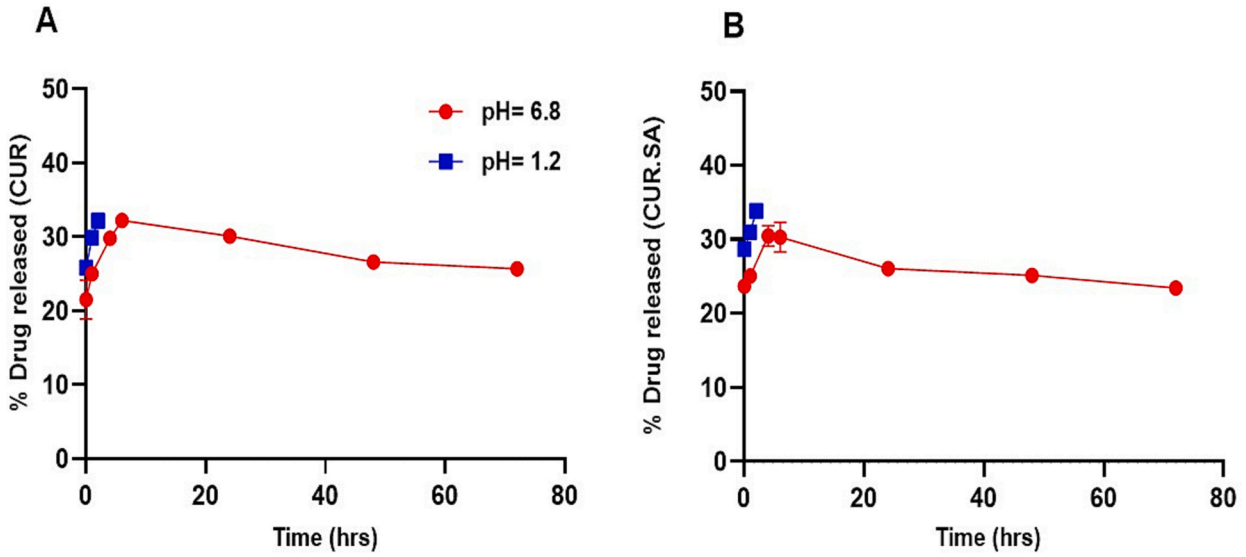

Fig. 8. In vitro drug release profiles of the prepared CUR-NPs (A); and CUR.SA-NPs (B) at pH 6.8 and pH 1.2. Data is expressed as mean ± SD (n = 3).

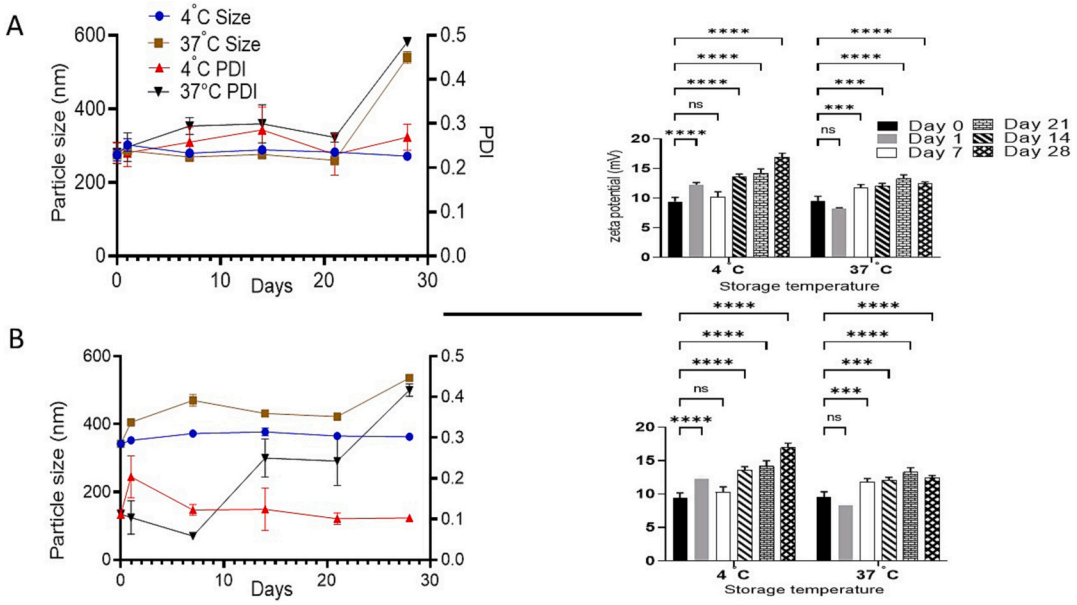

Fig. 9. Physical properties of (A) CUR-NPs; (B) CUR.SA-NPs as a function of a 28-day storage at 4 °C and 37 °C. Data expressed as mean ± SD and compared using two-way ANOVA, Dunnett's test, (ns = not significant, *$p < 0.05$, **$p < 0.01$ and ***$p < 0.001$, and ****$p < 0.0001$ indicates statistical significance compared to control cells (time 0)).

interests or personal relationships that could have appeared to influence the work reported in this paper.

Data availability

Data will be made available on request.

Acknowledgment

This work was supported by Qatar University Grant No IRCC-2021-006. Authors acknowledge the Central Laboratory Unit and Center of Advanced Materials, Qatar University for support in sample analyses.

References

Ahmadi, F., Ghasemi-Kasman, M., Ghasemi, S., Tabari, M. G., Pourbagher, R., Kazemi, S., & Alinejad-Mir, A. (2017). Induction of apoptosis in HeLa cancer cells by an ultrasonic-mediated synthesis of curcumin-loaded chitosan-alginate-STPP nanoparticles. *International Journal of Nanomedicine, 12*, 8545–8556. https://doi.org/10.2147/IJN.S146516

Aibani, N., Rai, R., Patel, P., Cuddihy, G., & Wasan, E. K. (2021). Chitosan nanoparticles at the biological Interface: Implications for drug delivery. *Pharmaceutics, 13*(10), 1686. https://doi.org/10.3390/pharmaceutics13101686

Babu, N. J., & Nangia, A. (2011). Solubility advantage of amorphous drugs and pharmaceutical cocrystals. *Crystal Growth and Design, 11*(7), 2662–2679. https://doi.org/10.1021/cg200492w

Baskaran, R., Madheswaran, T., Sundaramoorthy, P., Kim, H. M., & Yoo, B. K. (2018). Entrapment of curcumin into monoolein-based liquid crystalline nanoparticle dispersion for enhancement of stability and anticancer activity. *International Journal of Nanomedicine, 9*(1), 3119–3130. https://doi.org/10.2147/IJN.S61823

Del Castillo, M. L. R., López-Tobar, E., Sanchez-Cortes, S., Flores, G., & Blanch, G. P. (2015). Stabilization of curcumin against photodegradation by encapsulation in gamma-cyclodextrin: A study based on chromatographic and spectroscopic (Raman and UV-visible) data. *Vibrational Spectroscopy, 81*, 106–111. https://doi.org/10.1016/j.vibspec.2015.10.008

Chaubey, P., & Mishra, B. (2014). Mannose-conjugated chitosan nanoparticles loaded with rifampicin for the treatment of visceral leishmaniasis. *Carbohydrate Polymers, 101*(1), 1101–1108. https://doi.org/10.1016/j.carbpol.2013.10.044

Chaubey, P., Mishra, B., Mudavath, S. L., Patel, R. R., Chaurasia, S., Sundar, S., Suvarna, V., & Monteiro, M. (2018). Mannose-conjugated curcumin-chitosan nanoparticles: Efficacy and toxicity assessments against Leishmania donovani. *International Journal of Biological Macromolecules, 111*, 109–120. https://doi.org/10.1016/j.ijbiomac.2017.12.143

Chaubey, P., Patel, R. R., & Mishra, B. (2014). Development and optimization of curcumin-loaded mannosylated chitosan nanoparticles using response surface methodology in the treatment of visceral leishmaniasis. *Expert Opinion on Drug Delivery, 11*(8), 1163–1181. https://doi.org/10.1517/17425247.2014.917076

Dhanasekaran, S., Rameshthangam, P., Venkatesan, S., Singh, S. K., & Vijayan, S. R. (2018). In vitro and in silico studies of chitin and chitosan based nanocarriers for curcumin and insulin delivery. *Journal of Polymers and the Environment, 26*(10), 4095–4113. https://doi.org/10.1007/s10924-018-1282-8

Domenici, L., Monti, M., Bracchi, C., Giorgini, M., Colagiovanni, V., Muzii, L., & Benedetti Panici, P. (2016). D-mannose: A promising support for acute urinary tract infections in women. A pilot study. *European Review for Medical and Pharmacological Sciences, 20*(13), 2920–2925.

Ejaz, S., Ihsan, A., Noor, T., Shabbir, S., & Imran, M. (2020). Mannose functionalized chitosan nanosystems for enhanced antimicrobial activity against multidrug resistant pathogens. *Polymer Testing, 91*. https://doi.org/10.1016/j.polymertesting.2020.106814

Ficai, D., Albu, M. G., Sonmez, M., Ficai, A., & Andronescu, E. (2016). Advances in the field of soft tissue engineering: From pure regenerative to integrative solutions. In *Nanobiomaterials in Soft Tissue Engineering: Applications of Nanobiomaterials*. Elsevier Inc.. https://doi.org/10.1016/B978-0-323-42865-1.00013-1

Asher, G. N., & Spelman, K. (2013). Clinical utility of curcumin extract clinical utility of curcumin extract. *Alternative Therapies in Health and Medicine, 19*(2), 20–22. https://pubmed.ncbi.nlm.nih.gov/23594449/.

Asthana, G., Asthana, A., Kholi, D., & S. V.. (2021). Mannosylated chitosan nanoparticles for delivery of antisense oligonucleotides for macrophage targeting. *BioMed Research International, 2021*. https://doi.org/10.1155/2021/1878130

Han, J., Chen, F., Gao, C., Zhang, Y., & Tang, X. (2020). Environmental stability and curcumin release properties of Pickering emulsion stabilized by chitosan/gum arabic nanoparticles. *International Journal of Biological Macromolecules, 157*, 202–211. https://doi.org/10.1016/j.ijbiomac.2020.04.177

Hao, T., Wang, K., Zhang, S., Yang, S., Wang, P., Gao, F., Zhao, Y., Guo, N., & Yu, P. (2020). European journal of medicinal chemistry preparation, characterization, antioxidant evaluation of new curcumin derivatives and effects of forming HSA-bound nanoparticles on the stability and activity. *European Journal of Medicinal Chemistry, 207*, 0223–5234. https://doi.org/10.1016/j.ejmech.2020.112798

Kamaraj, S., Palanisamy, U. M., Kadhar Mohamed, M. S. B., Gangasalam, A., Maria, G. A., & Kandasamy, R. (2018). Curcumin drug delivery by vanillin-chitosan coated with calcium ferrite hybrid nanoparticles as carrier. *European Journal of Pharmaceutical Sciences, 116*(April 2017), 48–60. https://doi.org/10.1016/j.ejps.2018.01.023

Kumari, M., Sharma, N., Manchanda, R., Gupta, N., Syed, A., Bahkali, A. H., & Nimesh, S. (2021). PGMD/curcumin nanoparticles for the treatment of breast cancer. *Scientific Reports, 11*(1), 1–17. https://doi.org/10.1038/s41598-021-81701-x

Le, T. T., & Kim, D. (2019). Folate-PEG/Hyd-curcumin/C18-g-PSI micelles for site specific delivery of curcumin to colon cancer cells via Wnt/β-catenin signaling pathway. *Materials Science and Engineering C, 101*(September 2018), 464–471. https://doi.org/10.1016/j.msec.2019.03.100

Lestari, M. L. A. D., & Indrayanto, G. (2014). Curcumin. In. *Profiles of Drug Substances, Excipients and Related Methodology, 39*. https://doi.org/10.1016/B978-0-12-800173-8.00003-9

Mbese, Z., Khwaza, V., & Aderibigbe, B. A. (2019). Curcumin and Its Derivatives as Potential Therapeutic Agents in Prostate, Colon and Breast Cancers. *Molecules (Basel, Switzerland), 24*(23). https://doi.org/10.3390/molecules24234386

Nair, R. S., Morris, A., Billa, N., & Leong, C. O. (2019). An evaluation of curcumin-encapsulated chitosan nanoparticles for transdermal delivery. *AAPS PharmSciTech, 20*(2), 1–13. https://doi.org/10.1208/s12249-018-1279-6

Petković, M. (2012). O-H stretch in phenol and its hydrogen-bonded complexes: Band position and relaxation pathways. *Journal of Physical Chemistry A, 116*(1), 364–371. https://doi.org/10.1021/jp209897y

Pooresmaeil, M., & Namazi, H. (2020). Facile preparation of pH-sensitive chitosan microspheres for delivery of curcumin; Characterization, drug release kinetics and evaluation of anticancer activity. *International Journal of Biological Macromolecules, 162*, 501–511. https://doi.org/10.1016/j.ijbiomac.2020.06.183

Rodrigues, F. C., Anil Kumar, N. V., & Thakur, G. (2019). Developments in the anticancer activity of structurally modified curcumin: An up-to-date review. *European Journal of Medicinal Chemistry, 177*, 76–104. https://doi.org/10.1016/j.ejmech.2019.04.058

Samrot, A. V., Burman, U., Philip, S. A., Shobana, N., & Chandrasekaran, K. (2018). Synthesis of curcumin loaded polymeric nanoparticles from crab shell derived chitosan for drug delivery. *Informatics in Medicine Unlocked, 10*, 159–182. https://doi.org/10.1016/j.imu.2017.12.010

Saranya, T. S., Rajan, V. K., Biswas, R., Jayakumar, R., & Sathianarayanan, S. (2018). Synthesis, characterisation and biomedical applications of curcumin conjugated chitosan microspheres. *International Journal of Biological Macromolecules, 110*, 227–233. https://doi.org/10.1016/j.ijbiomac.2017.12.044

Shi, G. N., Zhang, C. N., Xu, R., Niu, J. F., Song, H. J., Zhang, X. Y., Wang, W. W., Wang, Y. M., Li, C., Wei, X. Q., & Kong, D. L. (2017). Enhanced antitumor immunity by targeting dendritic cells with tumor cell lysate-loaded chitosan nanoparticles vaccine. *Biomaterials, 113*, 191–202. https://doi.org/10.1016/j.biomaterials.2016.10.047

Song, W., Lee, B. H., Tan, L. P., & Li, H. (2019). Cardiovascular engineering materials in translational medicine. In *Biomaterials in Translational Medicine*. Elsevier Inc.. https://doi.org/10.1016/B978-0-12-813477-1.00004-9

Sorasitthiyanukarn, F. N., Muangnoi, C., Rojsitthisak, P., & Rojsitthisak, P. (2021). Chitosan-alginate nanoparticles as effective oral carriers to improve the stability, bioavailability, and cytotoxicity of curcumin diethyl disuccinate. *Carbohydrate Polymers, 256*. https://doi.org/10.1016/j.carbpol.2020.117426

Tang. (2017). Mannose metabolism: more than meets the eye, 2005 *Biochem Biophys Res Commun, 23*(1), 1–7. https://doi.org/10.1016/j.bbrc.2014.06.021.MANNOSE.

Tarhini, M., Badri, W., Greige-Gerges, H., Fessi, H., & Elaissari, A. (2021). Nanoparticles/nanoplatform to carry and deliver the drug molecules to the target site. *Drug Delivery Devices and Therapeutic Systems, 249–266*. https://doi.org/10.1016/b978-0-12-819838-4.00009-2

Tomeh, M. A., Hadianamrei, R., & Zhao, X. (2019). A review of curcumin and its derivatives as anticancer agents. *International Journal of Molecular Sciences, 20* (1033). https://doi.org/10.3390/ijms20051033

Ubeyitogullari, A., & Ciftci, O. N. (2019). A novel and green nanoparticle formation approach to forming low-crystallinity curcumin nanoparticles to improve curcumin's bioaccessibility. *Scientific Reports, 9*(1), 1–11. https://doi.org/10.1038/s41598-019-55619-4

Upadhyay, A., Gautam, S., Ramu, V., Kondaiah, P., & Chakravarty, A. R. (2019). Photocytotoxic cancer cell-targeting platinum(ii) complexes of glucose-appended curcumin and biotinylated 1,10-phenanthroline. *Dalton Transactions, 48*(47), 17556–17565. https://doi.org/10.1039/c9dt03490k

Valencia, M. S., da Silva Júnior, M. F., Xavier-Júnior, F. H., Veras, B.d. O., Albuquerque, P. B. S.d., Borba, E. F.d. O., … Carneiro-da-Cunha, M.d. G. (2021). Characterization of curcumin-loaded lecithin-chitosan bioactive nanoparticles. *Carbohydrate Polymer Technologies and Applications, 2*, Article 100119. https://doi.org/10.1016/j.carpta.2021.100119

Villegas-Peralta, Y., López-Cervantes, J., Madera Santana, T. J., Sánchez-Duarte, R. G., Sánchez-Machado, D. I., Martínez-Macías, M.d. R., & Correa-Murrieta, M. A. (2021). Impact of the molecular weight on the size of chitosan nanoparticles: characterization and its solid-state application. *Polymer Bulletin, 78*(2), 813–832. https://doi.org/10.1007/s00289-020-03139-x

Wichitnithad, W., Nimmannit, U., Wacharasindhu, S., & Rojsitthisak, P. (2011). Synthesis, characterization and biological evaluation of succinate prodrugs of curcuminoids for colon cancer treatment. *Molecules, 16*(2), 1888–1900. https://doi.org/10.3390/molecules16021888

Willenbacher, E., Khan, S. Z., Mujica, S. C. A., Trapani, D., Hussain, S., Wolf, D., Willenbacher, W., Spizzo, G., & Seeber, A. (2019). Curcumin: New insights into an ancient ingredient against cancer. *International Journal of Molecular Sciences, 20*(8), 1–13. https://doi.org/10.3390/ijms20081808

Xiao, J., Nian, S., & Huang, Q. (2015). Assembly of kafirin/carboxymethyl chitosan nanoparticles to enhance the cellular uptake of curcumin. *Food Hydrocolloids, 51*, 166–175. https://doi.org/10.1016/j.foodhyd.2015.05.012

Xiong, M., Lei, Q., You, X., Gao, T., Song, X., Xia, Y., Ye, T., Zhang, L., Wang, N., & Yu, L. (2017). Mannosylated liposomes improve therapeutic effects of paclitaxel in colon cancer models. *Journal of Microencapsulation, 34*(6), 513–521. https://doi.org/10.1080/02652048.2017.1339739

Yi, C., Qianming, D., Qianqian, G., Jing, H., Lina, L., Xiangchun, S., & Jianqing, P. (2018). A W/O emulsion mediated film dispersion method for curcumin encapsulated pH-sensitive liposomes in the colon tumor treatment. *Drug Development and Industrial Pharmacy*. https://doi.org/10.1080/03639045.2018.1539099

Zheng, B., & Mcclements, D. J. (2020). Formulation of more efficacious curcumin delivery systems using colloid science: Enhanced solubility, and bioavailability. *Molecules*, 1–25.